Received: 10 May 2021 | Revised: 31 August 2021 | Accepted: 4 September 2021

DOI: 10.1002/stc.2854

RESEARCH ARTICLE

WILEY

Restrictions and obstructions detection in pipe networks using incomplete and noisy flow and pressure steady-state measurements

Matteo Mazzotti[1] | **Mohanad Khazaali**[2] | **Paolo Bocchini**[2] | **Alberto Di Lullo**[3] | **Alessandro Marzani**[4]

[1]P. M. Rady Department of Mechanical Engineering, University of Colorado Boulder, Boulder, Colorado, USA

[2]Department of Civil and Environmental Engineering, Lehigh University, Bethlehem, Pennsylvania, USA

[3]Technology, R&D and Digital – TAOK, Eni SpA, San Donato Milanese, Italy

[4]Department of Civil, Chemical, Environmental and Materials Engineering - DICAM, University of Bologna, Bologna, Italy

Correspondence
Alessandro Marzani, Department of Civil, Chemical, Environmental and Materials Engineering - DICAM, University of Bologna, Viale Risorgimento 2, Bologna, Italy.
Email: alessandro.marzani@unibo.it

Funding information
Ente Nazionale Idrocarburi - Eni SpA (Italian Hydrocarbon Company)

Summary

Pipe networks for both water and oil distribution are prone to the formation of restrictions and, if not managed, possible obstructions. These reduce the efficiency of pipe systems and, in turn, cause negative economic impacts, temporary losses of service, and environmental risks. The present work focuses on a noninvasive methodology for the detection of restrictions in pipe networks. Restrictions are identified by minimizing, via genetic algorithms, a function that represents the discrepancy between on-field measured data and those simulated numerically. Measured data consist of a limited set of steady-state pressure heads and flow rates, which are the most commonly available information for pipe networks. The outcome of the technique is the "equivalent residual diameter" of each pipe in the network. This parameter allows the company managing the pipe network to identify the pipe segments where restrictions are most likely to be present and require further investigations. The approach is numerically validated for 15 different scenarios, considering five different sets of available measures and three different restriction conditions, in a mixed branched-looped network with complex topology for crude-oil transportation. The results show that the presence of restrictions is clearly identified and their magnitude is generally assessed with an accuracy of 5%.

KEYWORDS

genetic algorithms, inverse problems, obstructions, pipelines, pipe networks, restrictions, system identification

1 | INTRODUCTION

Restrictions, often due to deposits, are a typical problem in pipelines and pipe networks for the distribution of water and oil. The formation of restrictions is related to fluid composition, environmental conditions, and network topology, but almost all pipe systems can be affected by this issue. As a result, the pipe presents a reduced cross-sectional area, a variation of the cross-section shape, and frequently higher roughness compared to the original pipe. This, in turn, may

cause reduced flow capacity, negative economic impacts, temporary losses of service, and environmental risks. Hence, the prompt detection of restrictions in their early stages is of paramount importance for the pipe systems owners and operators as well as for the communities served.

Several procedures have been proposed in the past to detect restrictions in individual pipes and in pipe networks. The friction loss technique allows to detect restrictions along a pipe by observing changes of flows and pressures in time. This technique has been successfully applied to monitor the wax deposit in the Valhall subsea pipelines,[1] as well as to provide an indication of the diameter reduction caused by paraffin in laboratory tests.[2] The back-pressure method[3,4] enables the detection of restrictions in individual pipes by comparing the inlet–outlet pressure and the flow rate with the theoretical performance curve (pressure drop versus flow rate) of the pipe. Deviations from this curve observed during multirate tests can be related to the overall size of the restriction. The friction loss technique coupled with the mass balance method[5] allows the detection and characterization of a restriction in looped flow lines by performing frictional and volumetric tests. Moreover, using this method, the minimum detectable size of a restriction can be estimated a priori. However, these volumetric tests require that the investigated pipeline is isolated and the flow deviated. These conditions are rarely suitable for industrial pipelines in operation. Chen et al[6] discussed the application of an energy balance technique to determine the thickness of a paraffin deposit in laboratory test sections. This method considers the changes in heat transfer resulting from the restriction. However, as stated by the authors, this method works well in laboratory conditions, but its application in the field is limited to cases where both the inlet and outlet temperatures of the circulated fluid are above the ambient temperature. Hoffman and Amundsen[4] proposed a method based on the measurement of the weight increase of a pipeline segment due to a wax deposit. Although this method can reliably identify the residual diameter due to the obstruction, it requires the pipeline to be accessible and completely drained, while the mass density of the wax deposit needs to be known a priori. Methods that require minor interventions on the pipeline's operating conditions have been presented in Guillén et al. and Besançon et al,[7,8] where finite-difference-based flow models that use pressure heads and flow rates measurements under different steady-state flow regimes are used to identify the location and reduced section due to a restriction.

Multirate flow tests in conjunction with flow, pressure, and temperature data have also been used to locate and quantify restrictions in single-phase gas pipelines by assuming that it occurs at only one location.[9] Recently, flow models for restriction detection have also been proposed in which the extended Kalman filter is used to produce an estimate of the restriction size and location from the knowledge of inlet and outlet flow and pressure head in a pipeline.[10,11]

All the steady-state-based techniques mentioned above have been developed and tested for single pipelines, which makes them not efficient or cost-effective for restriction monitoring at the network scale. Similarly, most of the available methodologies for restrictions detection are based on the measurement of the transient response of the pipeline[12–18] or the fluid[19–30] to a dynamic impulse. However, their application to extensive pipe networks requires the deployment of specific equipment over the entire system,[15,16,31] whereas in many situations, it might be desirable to utilize available operational steady-state data.

For this reason, a two-step multiscale approach is proposed. The first step focuses at the network scale and aims at identifying the pipelines affected by restrictions using measurements easy to obtain and compatible with the normal operational conditions of the network.

The identification of potential restrictions triggers the second step, where more sophisticated measurements and procedures are applied to the individual pipes in order to locate the restrictions and eventually remove them.

As several techniques are already available to perform the second step, as those recalled in this introduction, this paper proposes a noninvasive method to accomplish the first step. In particular, the technique proposed in this paper achieves the following goals: (i) identify restrictions on entire pipe networks; (ii) Quantify the extent of the restrictions in terms of equivalent residual diameters; (iii) use only measures that are easily obtained under normal operational conditions; and (iv) be effective with a limited number of noisy measurements.

The proposed method detects partial restrictions in pipe networks by using only steady-state data of nodal pressure heads and pipe flows, which are the quantities most commonly measured during the normal operation of the network. Furthermore, it exploits redundant information to reduce the number of measures that would be necessary to apply the previously listed methodologies to each individual pipe.

This approach was developed some years ago in collaboration with the Italian Energy Company (Eni SpA)[32] and illustrated on few ideal and theoretical cases only.[32,33] Still, its feasibility in complex pipe networks considering scarce measurements was never tested nor disseminated. Thus, here we show its application to a complex looped and

branched network, representative of a true pipe network for crude oil transportation, considering several restrictions scenarios and missing measurements along with a detailed accuracy analysis.

Restrictions are identified by minimizing the discrepancy between the available measures and those simulated by an ad-hoc developed finite element model (FEM) of the pipe network. The fundamental design variable of the optimization problem is the equivalent diameter of each pipe in the network, which is defined herein as the diameter of a uniform pipe that generates a pressure drop equivalent to that of the potentially restricted or obstructed pipe. From a mathematical point of view, the equivalent diameter is calculated from the concept of pipes in series by splitting a single pipeline into two or more segments, one of which represents the restriction of unknown length and reduced diameter. This modeling approach allows the detection of a restriction and the quantitative assessment of its extent. The optimization problem is solved by means of genetic algorithms (GAs), which do not need a reasonable initial guess, can easily handle multiple local minima (common in pipe network problems), and do not require the objective function to be continuous or differentiable.[34] The idea of solving identification problems by updating the parameters of a FEM using GAs is relatively common in the literature.[35–40] Hence, some of the findings of this research in terms of objective functions, identification under missing measurements, and sensitivity based on the topology of the system can be extended to formally similar problems in other engineering fields.

2 | PROPOSED METHODOLOGY

2.1 | Pipeline network model for steady-state flow

The analysis of the steady-state flow for pipe networks presented in the following is based on the finite element like scheme proposed by Mohtar et al.[41] which is extended to account for the dependency on temperature, density, and dynamic viscosity of the carried fluid.

Using the concept of pipes in series, the total frictional (distributed) head loss for a restricted pipe element as shown in Figure 1 is calculated by considering a pipe of equivalent diameter, which is defined as the diameter of a uniform pipe that has the same head loss of the real pipe. It follows that, by using only steady-state data of pressure and flow rate, restrictions are detectable and quantifiable in terms of equivalent diameter reduction, but not in terms of length of the restrictions and actual residual diameters. As it is well known,[42] a system of several pipe segments in series with different lengths L_j, diameters D_j, and comparable friction factors can be seen as a single pipeline with total length $\sum_j L_j$ and equivalent uniform diameter:

$$\hat{D} = \left[\frac{\sum_j L_j}{\sum_j L_j / D_j^5} \right]^{1/5}. \tag{1}$$

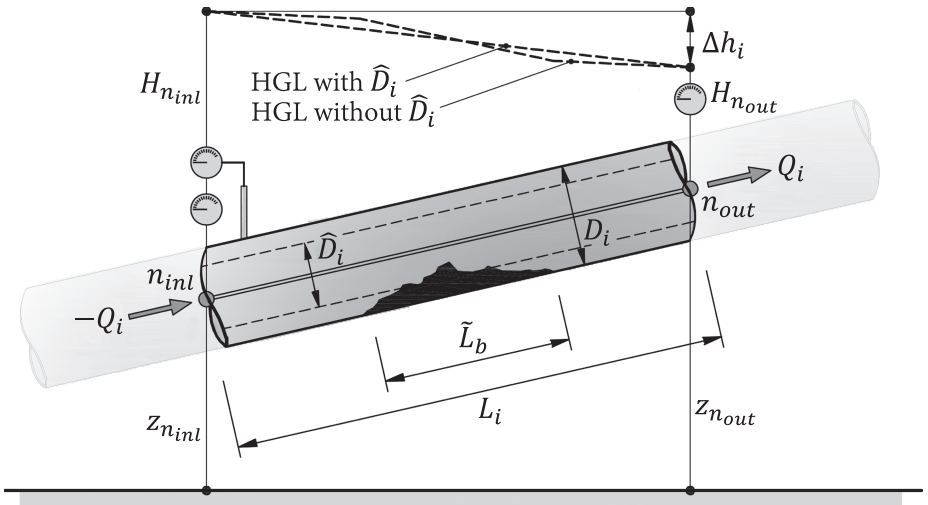

FIGURE 1 Schematic representation of the obstructed pipeline finite element

Therefore, the partially obstructed pipe i in Figure 1 can be modeled as two pipes in series: the first with length equal to the length of the unobstructed portion of the pipe (i.e., $L_i - \tilde{L}_b$) and diameter equal to the design diameter D_i and the second with length and diameter equal to the restriction length $\tilde{L}_b$ and the residual diameter in the blocked portion $\tilde{D}_b$, respectively. For the purpose of the identification procedure, the equivalent diameter reduction is modeled via a dimensionless factor:

$$\alpha_i = \frac{\hat{D}_i}{D_i},\ \alpha_i \in [0,1]. \tag{2}$$

so that $\alpha_i = 0$ indicates that the ith pipe is totally obstructed, whereas $\alpha_i = 1$ denotes a full-bore pipe. Figure 2 shows how different combinations of blockage length $\tilde{L}_b$ and residual diameter $\tilde{D}_b$ can lead to the same value of α.

With reference to Figure 1 and by using the Darcy–Weisbach formula[42] along with the energy conservation theorem[41] and Equation (2), the equation of the hydraulic grade line (indicated as HGL in Figure 1) for the ith pipe element of constant diameter $\hat{D}_i = \alpha_i D_i$ connecting an inlet node n_{inl} (elevation $z_{n_{inl}}$ and pressure head $H_{n_{inl}}$) and an outlet node n_{out} (elevation $z_{n_{out}}$ and pressure head $H_{n_{out}}$) can be computed as follows:

$$\Delta h_i(\alpha_i) = (z_{n_{inl}} - z_{n_{out}}) + (H_{n_{inl}} - H_{n_{out}}) = k_i(\alpha_i) Q_i^2, \tag{3}$$

where Q_i denotes the volumetric flow rate in the pipe while the frictional loss coefficient $k_i(\alpha_i)$ is given by:

$$k_i(\alpha_i) = \frac{8 f_i(\alpha_i, Q_i, \tau_i) L_i}{\pi^2 g \alpha_i^5 D_i^5}, \tag{4}$$

in which g stands for the gravitational acceleration and $f_i(\alpha_i, Q_i, \tau_i)$ denotes the friction factor. The latter is a function of the flow rate Q_i and average temperature τ_i and is computed from the Chen's formula[2] as follows:

$$f_i(\alpha_i, Q_i, \tau_i) = -2.0 \log\left\{ \frac{e_i}{3.7065(\alpha_i D_i)} - \frac{5.0452}{\mathrm{Re}(\alpha_i, Q_i, \tau_i)} \log\left[\frac{e_i^{1.1098}}{2.8257(\alpha_i D_i)^{1.1098}} + \frac{5.8506}{[\mathrm{Re}(\alpha_i, Q_i, \tau_i)]^{0.8981}} \right] \right\}, \tag{5}$$

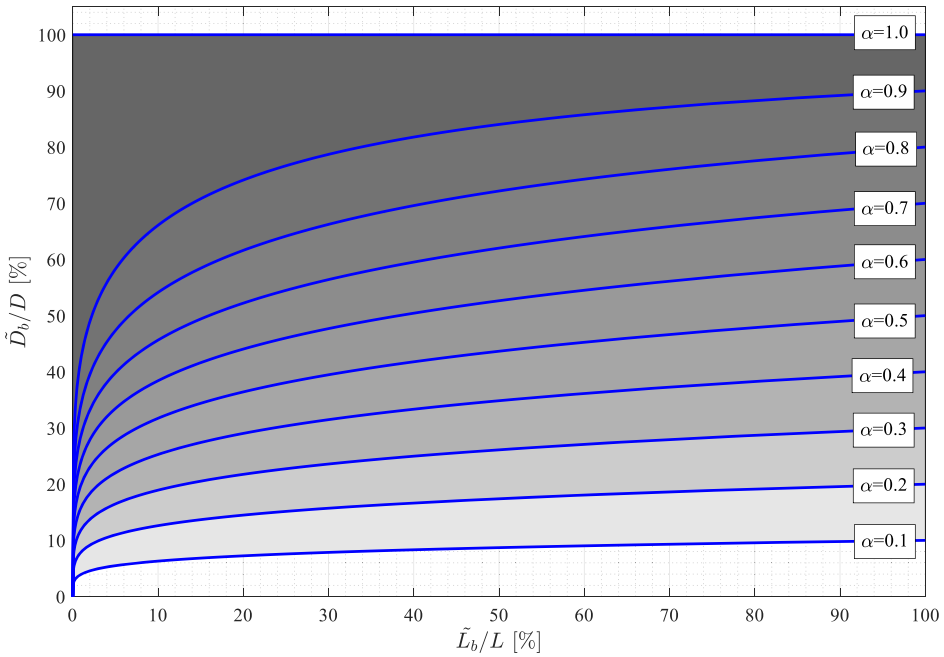

FIGURE 2 Comparison of different combinations of blockage length and residual diameter that result in the same value of α

where e_i denotes the pipe roughness, $\mathrm{Re}(\alpha_i, Q_i, \tau_i) = 4\rho(\tau_i)Q_i/(\pi^2\alpha_i^2 D_i^2 \mu(\tau_i))$ indicates the Reynolds number while $\rho(\tau_i)$ and $\mu(\tau_i)$ denote the temperature-dependent mass density and dynamic viscosity of the fluid, respectively. Such properties can be retrieved from databases[43] or experimentally determined. In this work, the temperature τ_i is assumed to be independent from the volumetric flow rate and is only used to define the fluid properties in the ith pipe.

Following the approach proposed by Mohtar et al,[41] a system of nonlinear algebraic equations satisfying the mass balance at all the N_N nodes of a network with N_P pipes can be written in the form:

$$\mathbf{R}(\mathbf{H}(\boldsymbol{\alpha})) = \mathbf{Q}_I(\mathbf{H}(\boldsymbol{\alpha})) + \mathbf{Q}_E = \mathbf{0}, \tag{6}$$

where $\mathbf{Q}_E = \{Q_{E,1}, .., Q_{E,N_N}\}^{\mathrm{T}}$ is a global vector of external inlets or outlets while $\mathbf{Q}_I(\mathbf{H}(\boldsymbol{\alpha})) = \{Q_{I,1}, .., Q_{I,N_N}\}^{\mathrm{T}}$ collects the nodal loads due to internal flow circulation, which are self-equilibrated in absence of external inflows or outflows. The latter are a function of the nodal pressure heads $\mathbf{H}(\boldsymbol{\alpha}) = \{H_1(\boldsymbol{\alpha}), .., H_{N_N}(\boldsymbol{\alpha})\}^{\mathrm{T}}$ as well as the normalized equivalent diameters $\boldsymbol{\alpha} = \{\alpha_1, .., \alpha_{N_P}\}^{\mathrm{T}}$ (i.e., the objectives of the identification procedure), and are expressed as follows:

$$\mathbf{Q}_I(\mathbf{H}(\boldsymbol{\alpha})) = \mathop{\mathrm{A}}_{i=1}^{N_P} c_i(\alpha_i) \begin{Bmatrix} \Delta h_i(\alpha_i) \\ -\Delta h_i(\alpha_i) \end{Bmatrix}, \tag{7}$$

where $\mathrm{A}_{i=1}^{N_P}$ represents an element-wise assembly operation and the coefficients $c_i(\alpha_i)$ read:

$$c_i(\alpha_i) = [k_i(\alpha_i)|\Delta h_i(\alpha_i)|]^{-1/2}. \tag{8}$$

The solution of Equation (6) can be found in terms of pressure heads $\mathbf{H}(\boldsymbol{\alpha})$ and associated nodal loads $\mathbf{Q}_I(\mathbf{H}(\boldsymbol{\alpha}))$ by applying the Newton–Raphson algorithm.[44] The algorithm reconstructs $\mathbf{H}(\boldsymbol{\alpha})$ from the iterative sequence:

$$\mathbf{H}_{r+1}(\boldsymbol{\alpha}) = \mathbf{H}_r(\boldsymbol{\alpha}) - \left[\left(\frac{\partial \mathbf{R}(\mathbf{H}(\boldsymbol{\alpha}))}{\partial \mathbf{H}} \right)_{\mathbf{H}=\mathbf{H}_r(\boldsymbol{\alpha})} \right]^{-1} \mathbf{R}(\mathbf{H}_r(\boldsymbol{\alpha})), \tag{9}$$

in which the gradient of the residual loads is given by

$$\frac{\partial \mathbf{R}(\mathbf{H}(\boldsymbol{\alpha}))}{\partial \mathbf{H}} = \mathop{\mathrm{A}}_{i=1}^{N_P} c_i^2(\alpha_i) \left(\begin{bmatrix} 1 & -1 \\ -1 & 1 \end{bmatrix} - \frac{1}{2} c_i(\alpha_i) \begin{bmatrix} \Delta h_i(\alpha_i) & -\Delta h_i(\alpha_i) \\ -\Delta h_i(\alpha_i) & \Delta h_i(\alpha_i) \end{bmatrix} \right). \tag{10}$$

In order to initiate the sequence in Equation (9), an initial guess of the friction coefficients $f_1, ..., f_{N_P}$ is required in addition to a tentative solution $\mathbf{H}_0(\boldsymbol{\alpha})$. At the rth iteration, the friction coefficients for the ith pipe are corrected by inverting Equation (3) using the solution at the previous step $\Delta h_i, r-1(\alpha_i)$ and substituting the resulting $Q_i(\alpha_i)$ into Equation (5). After the new set of friction coefficients has been evaluated, the current solution $\mathbf{H}_r(\boldsymbol{\alpha})$ is used to update the nodal loads and pressure heads from Equations (7) and (9), respectively. The iterations are then repeated until the convergence criterion $\|\mathbf{H}_r(\boldsymbol{\alpha}) - \mathbf{H}_{r-1}(\boldsymbol{\alpha})\|_{L2} / \|\mathbf{H}_{r-1}(\boldsymbol{\alpha})\|_{L2} \leq 1.0^{-5}$ is met.

2.2 | Optimization framework based on GAs

The identification of partial restrictions a pipe network is formulated as an optimization problem. The objective function to be minimized is a metric of the discrepancy between measured (Q^{exp} and H^{exp}) and numerically simulated (Q^{sim} and H^{sim}) pipe flow rates and nodal pressure heads. Simulated data are obtained by the FEM formulation described in Section 2.1 for a given set w of pipeline diameters $\boldsymbol{\alpha}_w = \{\alpha_{w,1}, \alpha_{w,2}, ..., \alpha_{w,i}, ..., \alpha_{w,N_P}\}$.

The optimization problem is solved using GAs, which are a heuristic technique that performs a search based on evolutionary sets of trial solutions. The basic idea of GAs is to identify the optimal solution from a population of individuals that represent a set of potential (trial) solutions of the problem. By applying genetic operators, the solution evolves generation-by-generation to the global optimum.[34]

The proposed detection procedure can be summarized in the following steps:

1. An initial population of trial solutions ($\boldsymbol{\alpha}_1, \boldsymbol{\alpha}_2, \ldots \boldsymbol{\alpha}_{N_I}$) is generated. In the first generation of the GA procedure, one of these trials represents the case where no restrictions are present (i.e., $\alpha_{1,i} = 1 \,\forall i$), whereas all the remaining trials are generated randomly. All entries of all trials satisfy the lower and upper bounds of the solution space, that are set to 0 and 1, respectively.
2. For each individual $\boldsymbol{\alpha}_w$, the FEM described in Section 2.1 assembles Equation (6) and solves it by the Newton–Raphson scheme, providing the pressure head $H^{sim}(\boldsymbol{\alpha}_w)$ at every node and the flow rate $Q^{sim}(\boldsymbol{\alpha}_w)$ in every pipe of the network.
3. The fitness value of each individual $\boldsymbol{\alpha}_w$ is then calculated as follows:

$$J(\boldsymbol{\alpha}_w) = \log_{10}(\Phi_H) + \log_{10}(\Phi_Q) - \frac{\gamma}{N_P}\sum_{i=1}^{N_P}\alpha_{w,i}, \tag{11}$$

where

$$\Phi_H = \sum_{\nu=1}^{N_H}\left(\frac{H_\nu^{sim}(\boldsymbol{\alpha}_w) - H_\nu^{exp}}{H_\nu^{exp}}\right)^2, \tag{12}$$

$$\Phi_Q = \sum_{\nu=1}^{N_Q}\left(\frac{Q_\nu^{sim}(\boldsymbol{\alpha}_w) - Q_\nu^{exp}}{Q_\nu^{exp}}\right)^2, \tag{13}$$

in which H_ν^{exp} and Q_ν^{exp} are the data for the νth node and pipe, respectively. The variable N_H is the total number of measured pressure heads and N_Q the total number of measured flow rates. If some experimental measures are missing, N_H and N_Q will be smaller than the total number of nodes and the total number of pipes within the network, respectively. It can be noted that, although all the nodal pressure heads and pipe flow rates are computed numerically, the fitness is built by considering only the simulated data for which a corresponding experimental measure is available. The last term in Equation (11) is a penalization term added to reduce the likelihood of false restriction detection caused by experimental errors.[37,45] The penalization factor γ depends on the characteristics of the network and can be determined by numerical simulations, as explained in Section 3.3.

4. The population is sorted according to the fitness value of each individual. Next, the convergence criteria of the GAs scheme are checked. Since the proposed fitness function does not provide an inferior limit, the algorithm stops when no improvements in the best fitness values are observed for a preset number of generations or if the maximum number of generations is reached. If either of the convergence criteria is satisfied, the analysis is stopped, and the best individual obtained (i.e., $\boldsymbol{\alpha}_w$ such that $J(\boldsymbol{\alpha}_w)$ is minimum) is selected as the final solution $\boldsymbol{\alpha}^{ID}$.
5. If none of the convergence criteria is satisfied, a fixed number of $\boldsymbol{\alpha}_w$, those with the best fitness values, are directly passed to the next generation as "elite members," while a fraction of the remaining $\boldsymbol{\alpha}_w$, the so-called parent individuals, is selected from the population for the "reproduction." From the parent individuals, the crossover operator generates an offspring using a random binary vector called "mask." The offspring is formed by copying the bit of the first parent or that of the second parent according to the position in the mask of the numbers 0 and 1, respectively. The total number of parent individuals who generate offspring is defined through the crossover fraction, expressed as a percentage of the population size.
   Next, the "mutation" adds a random number chosen from a Gaussian distribution to each entry of the parent vector. The amount of mutation is decreased with each generation as the algorithm converges to the global minimum. The mutation ensures that a subset of the offspring is used to randomly scan the search space for possible better solutions. The overall amount of mutation is increased when several local minima are expected, as it is usually the case with noise-contaminated data.
6. Using the individuals of the new generation, the algorithm restarts from Point 2, and the procedure continues until convergence is met.

A schematic flowchart of the proposed methodology is shown in Figure 3. The input of the algorithm consists in the characteristics of the pipe network (nodal coordinates and connectivity) and the individual pipes (length, design diameter, roughness, average temperature). In addition, the boundary conditions (wells/reservoirs and nodal inlets/outlets) and available measures in terms of pipe flows Q_ν^{exp} and nodal pressure heads H_ν^{exp} must also be provided. With the input data, the GA-based optimization procedure searches for the potential restrictions in the network by minimizing Equation (11) with respect to the normalized equivalent diameters α_i.

The solution of the identification process is, in general, not unique. The configuration of the system, the type, and number of collected data can lead to situations where multiple solutions are present. For some network topologies, increasing the number of measurements and using a sensitivity analysis like the one presented in Section 3.5 to increase their effectiveness may lead to a unique solution, but in some cases, the topology of the system and the boundary conditions can make nonunique solutions unavoidable (see for instance the discussion by Viola and Bocchini[39]). Moreover, measurement errors and model uncertainties may create additional local minima. For these reasons, in the following sections, the robustness of the proposed procedure will be discussed, for a different number of available measures and considering a realistic level of applied noise to simulate measurement errors and model uncertainties.

3 | NUMERICAL APPLICATION

3.1 | Description of the case study

To demonstrate the efficiency and effectiveness of the proposed method, the mixed branched-looped network for crude oil transportation shown in Figure 4, with 15 pipes and 15 nodes, is examined. The oil is extracted from the reservoirs, located at Nodes 7, 8, 9, 12, 13, 14, and 15, where a pressure head is imposed. The pressure head is also imposed at node 1, where the oil is collected. The network data are given in Tables 1 and 2.

As discussed in Section 2.1, the density and the dynamic viscosity of the oil in the ith pipe depend on the oil temperature τ_i. As each pipe of the network can be modeled by considering one or more pipe segments, the fluid properties

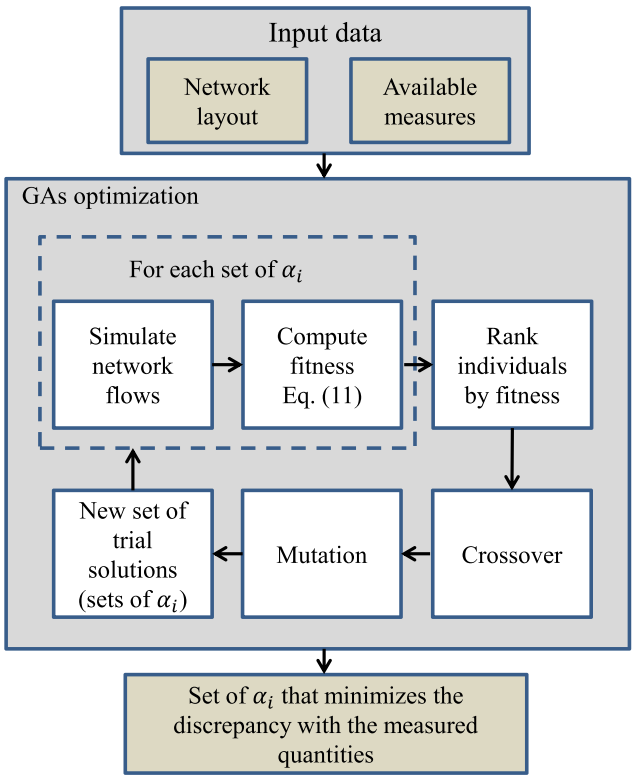

FIGURE 3 Flow-chart of the proposed methodology

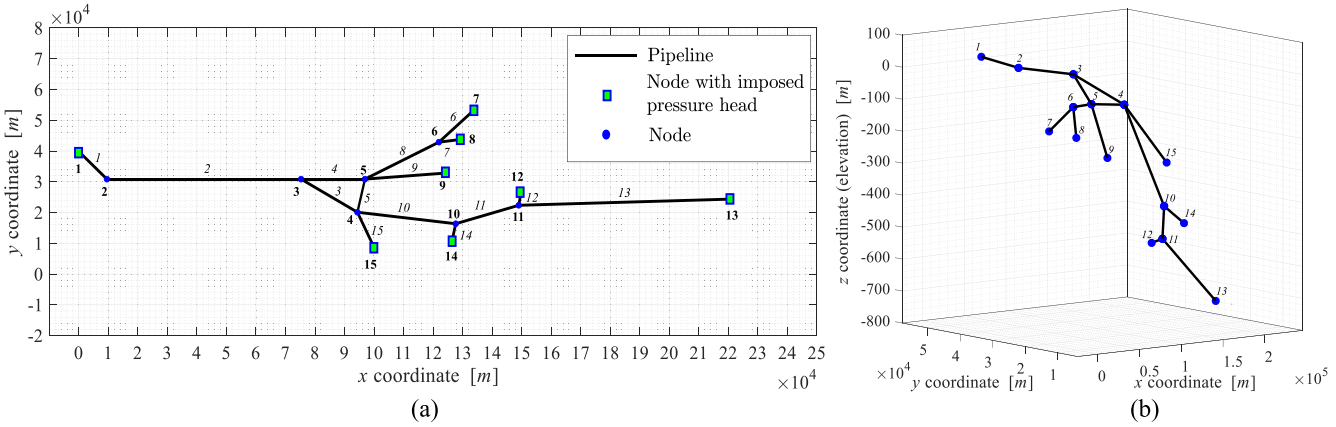

FIGURE 4 Network carrying crude oil. (a) Planar view. (b) Three-dimensional view; for the sake of clarity, the axes are plotted in different scales

TABLE 1 Nodal coordinates with imposed pressure heads and oil temperature

Node	x (m)	y (m)	z (m)	H (m)	τ (°C)
1	0	39,860	60	10	22.0
2	9,520	30,860	40	—	22.0
3	75,280	30,860	0	—	22.0
4	94,360	20,100	−80	—	20.2
5	96,920	30,860	−100	—	19.7
6	121,960	42,880	−140	—	18.8
7	133,900	53,380	−240	450	16.5
8	128,820	43,700	−240	450	16.5
9	123,680	32,800	−280	490	15.6
10	127,660	16,360	−400	—	12.8
11	149,000	22,360	−520	—	10.1
12	149,660	25,860	−540	790	9.6
13	220,660	24,360	−740	990	5.0
14	126,200	9,860	−440	690	11.9
15	100,080	8,500	−240	450	16.5

can vary along each pipe according to the given temperature distribution. In this application, as single pipe segments were used to connect two nodes of the network, the oil temperature in each pipe was taken as the mean between those at its inlet and outlet nodes. The oil temperature at nodes with $z \geq 0\ m$ has been considered equal to 22°C. For the underwater nodes, the temperature was assumed to vary linearly with the depth from 22°C at $z = 0$ m to 5°C for $z = -740$ m (node 13). The considered temperature at the nodes of the pipe network are given in Table 1. Next, the oil properties in each pipe were derived according to its mean temperature by interpolating the values given in Table 3.[46]

The numerical simulations are carried out on fifteen different cases generated by considering five different sets of available field measures (M1, M2, M3, M4, and M5) and three different restriction scenarios (B1, B2, and B3), as shown in Figure 5. The different sets of available measures used in the identifications and the modeled restrictions are also described in Tables 4 and 5, respectively. In the last column of Table 5, the equivalent normalized diameter of the ith restricted pipe has been indicated as α^{Ref}, where the superscript *Ref* denotes the reference value of α that has to be identified.

TABLE 2 Pipeline network properties

Pipe	Inlet node	Outlet node	L (m)	D (m)	e (mm)
1	1	2	13,101	0.40	0.5
2	2	3	65,760	0.40	0.5
3	3	4	21,905	0.35	0.5
4	3	5	21,640	0.35	0.5
5	4	5	11,060	0.35	0.5
6	6	7	15,900	0.30	0.5
7	6	8	6,910	0.30	0.5
8	6	5	27,776	0.30	0.5
9	5	9	26,831	0.30	0.5
10	4	10	33,511	0.35	0.5
11	10	11	22,168	0.35	0.5
12	11	12	3,562	0.30	0.5
13	11	13	71,688	0.30	0.5
14	10	14	6,662	0.30	0.5
15	4	15	12,935	0.30	0.5

TABLE 3 Density and dynamic viscosity of the oil at different temperatures

Elevation (m)	Temperature (°C)	Density (kg/m^3)	Dynamic viscosity (Pa·s)
≥0	22	829.17	0.0157
−740	5	874.82	0.0905

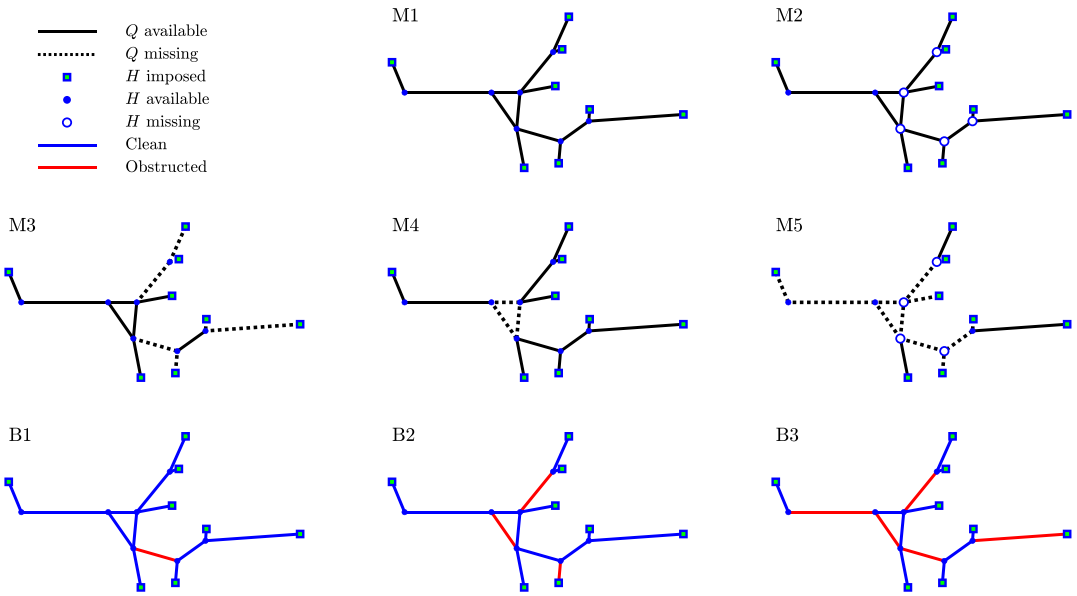

FIGURE 5 Missing measures (M1, M2, M3, M4, and M5) and restrictions (B1, B2, and B3) conditions for the pipe network in Figure 4. Fifteen scenarios are studied by combining each one of the five missing measures cases with the three restriction conditions. The aspect ratio of the network is out of scale for representation purposes

TABLE 4 Measurement cases with missing Q and H for the pipe networks in Figure 5

Measurement case	Pipe with missing Q	Nodes with missing H
M1	—	—
M2	—	4, 5, 6, 10, 11
M3	6, 7, 8, 10, 13, 14	—
M4	3, 4, 5	—
M5	1, 2, 3, 4, 5, 8, 9, 10, 11, 12, 14	4, 5, 6, 10

TABLE 5 Restrictions scenarios simulated for the pipe networks in Figure 4

restriction case	pipe	L (m)	D (m)	$\tilde{L}_b/L$ (%)	$\tilde{D}_b/D$ (%)	$\hat{D}$ (m)	α^{Ref}
B1	10	33,511	0.35	100	80	0.28	0.80
B2	3	21,905	0.35	100	80	0.28	0.80
	8	27,776	0.30	100	20	0.06	0.20
	14	6,662	0.30	100	80	0.24	0.80
B3	2	65,760	0.40	80	70	0.30	0.75
	3	21,905	0.35	60	80	0.30	0.87
	8	27,776	0.30	60	70	0.29	0.76
	10	33,511	0.35	50	80	0.30	0.85
	13	71,688	0.30	10	50	0.22	0.73

Note: $\tilde{L}_b/L$ and $\tilde{D}_b/D$ denote, for the ith pipe element in the second column, the percentage of restriction length and restriction residual diameter with respect to the design ones.

3.2 | Pseudo-experimental data

In absence of real field data, the accuracy of the proposed method is assessed by using pseudo-experimental data, which are generated as explained in the following. For a given restriction scenario, the flow rates Q_i and pressure heads H_n are first computed using the model described in Section 2.1. Then, to simulate measurement errors, these quantities are contaminated with random noise as follows:

$$Q_i^{exp} = Q_i(1 + M_Q \times \xi_i) \; \forall \, i \in \{1, N_P\}, \tag{14}$$

$$H_n^{exp} = H_n(1 + M_H \times \eta_n) \; \forall \, n \in \{1, N_N\}, \tag{15}$$

where M_Q and M_H are the noise levels for the flows and pressure heads, respectively, while ξ_i and η_n are independent random variables with a standard Gaussian distribution (i.e., zero mean and unit standard deviation). The sample values of ξ_i and η_n change from pipe to pipe and from node to node, respectively.

As described in Section 2.2, the system of nonlinear governing equations in Equation (6) is assembled and solved for all nodes and pipes in the network, whereas the fitness function is built using only entries for which corresponding pseudo-experimental measures are available.

3.3 | Restriction identifications

For the identification analyses a population of 2,000 individuals was used, whereas the maximum number of generations was set equal to 200. The number of elite members was set to 100 and the crossover fraction was assumed equal to 0.8. Finally, in the mutation operator, the standard deviation value in the first step of the procedure was set equal to

1. This value has not been assumed constant during the analysis, but it was linearly decreasing over the generations to reach the value 0 at the last generation. The penalization factor γ in Equation (11) was set equal to 17. In an extensive numerical investigation, such value consistently provided robustness and fast convergence for several restrinction scenarios. Finally, because Equation (11) does not provide an inferior limit, the convergence tolerance was set to be 10^{-13}.

In order to verify the robustness of the proposed method, the identification procedure was performed 30 times for each scenario, considering each time a different random noise for the pseudo-experimental data. In particular, 10% noise was assumed on the flow rates and 5% noise for all pressure head measurements, hence $M_Q = 10\%$ and $M_H = 5\%$, respectively. The added noise levels to the flow and pressure head measurements also account for the fact that the pipes roughness can change from pipe to pipe and over time (i.e., the uncertainty in pipes roughness), as well as other modeling errors.

Results are shown in Figure 6, where the bar represents the value of α^{Ref}, the large white circle indicates the median value of α^{ID} over the 30 repetitions associated with different pseudo-experimental measures, whereas the violin plot is used to show the probability density of α^{ID} over the 30 repetitions. Results are also collected in Table 6, where for each considered case and each pipe α^{Ref} is given along with the mean and coefficient of variation of the 30 identifications.

For each investigated scenario, the proposed procedure is capable of identifying the restricted pipe. In fact, the results show a very good correspondence between the target α^{Ref} parameters and those identified by the procedure, with average errors generally close to the noise level of the pseudo-experimental data. Furthermore, the coefficients of variation are mostly lower than 5%, with few exceptions for the cases in which α^{Ref} is very small.

In particular, the target scenario B1 (left column) is identified correctly for all the sets of available measures; the restriction in Pipe 10 is assessed with good accuracy and no false positives (i.e., $\alpha^{ID} < 1$ for clean pipes) are present.

It should be emphasized here that the restriction in Pipe 10 is correctly identified also for the M5 case, for which flows are given in three pipes only (the flow is unknown in Pipe 10) and pressures are measured at very few nodes.

The condition B2, characterized by three restricted pipes (3, 8, and 14), is correctly identified by using the M1 and M2 sets of input data. When sets M3, M4, or M5 are used as input, some of the obstructions are undetected. However, it can be noted that a restriction in a pipe is always detected when its flow measure is available, even in the absence of pressure heads at the inlet and outlet nodes. Similar results are also observed for the B3 case.

3.4 | Discussion of the results

A quantitative accuracy analysis is performed. A total of 6,750 values of α_i^{ID} were estimated (15 pipelines $\times$ 15 scenarios $\times$ 30 analyses with different noise). Two different errors for each scenario have been defined:

$$e_{s,i,m}^{ID} = \alpha_{s,i}^{Ref} - \alpha_{s,i,m}^{ID} \ \forall i \in \{\text{set of pipes with a restriction in scenario } s\},\ m \in \mathbb{N}(1,30), \tag{16}$$

$$e_{s,i,m}^{FP} = 1 - \alpha_{s,i,m}^{ID} \ \forall i \in \{\text{set of pipes without restriction in scenario } s\},\ m \in \mathbb{N}(1,30), \tag{17}$$

where the subscript m runs over the 30 analyses performed with different values of random noises on the measurements, ξ_i and η_n, while the subscript s indicates the scenario. The value of e^{ID} is the error of the procedure in identifying occluded pipes, and it can be calculated for 1,350 data points: nine restricted pipes (see Table 5 for each measurement case [M1, M2, M3, M4, M5] considered, with 30 analyses for each scenario). The value of e^{FP} is the error related to false positives, i.e., the error committed by the procedure in identifying clean pipes ($\alpha^{Ref} = 1$) as potentially restricted. In this case, 5,400 data points are available to assess the error (36 clean pipes $\times$ 5 measurement cases $\times$ 30 analyses). For instance, for scenario M2-B3, e^{ID} is calculated for Pipes 2, 3, 8, 10, and 13, where the restrictions are located, whereas e^{FP} is calculated for the clean pipes (i.e., 1, 4–7, 9, 11, 12, 14, and 15). The computed values of e^{ID} and e^{FP} for this scenario are shown in Figure 7.

The mean relative error e^{ME} over the 30 repetitions, calculated for each scenario and pipeline using Equation (18), is shown in Figure 8.

$$e_{s,i}^{ME} = \frac{1}{30}\sum_{m=1}^{30}\left|\frac{\alpha_{i,m}^{Ref} - \alpha_{i,m}^{ID}}{\alpha_{i,m}^{Ref}}\right|. \tag{18}$$

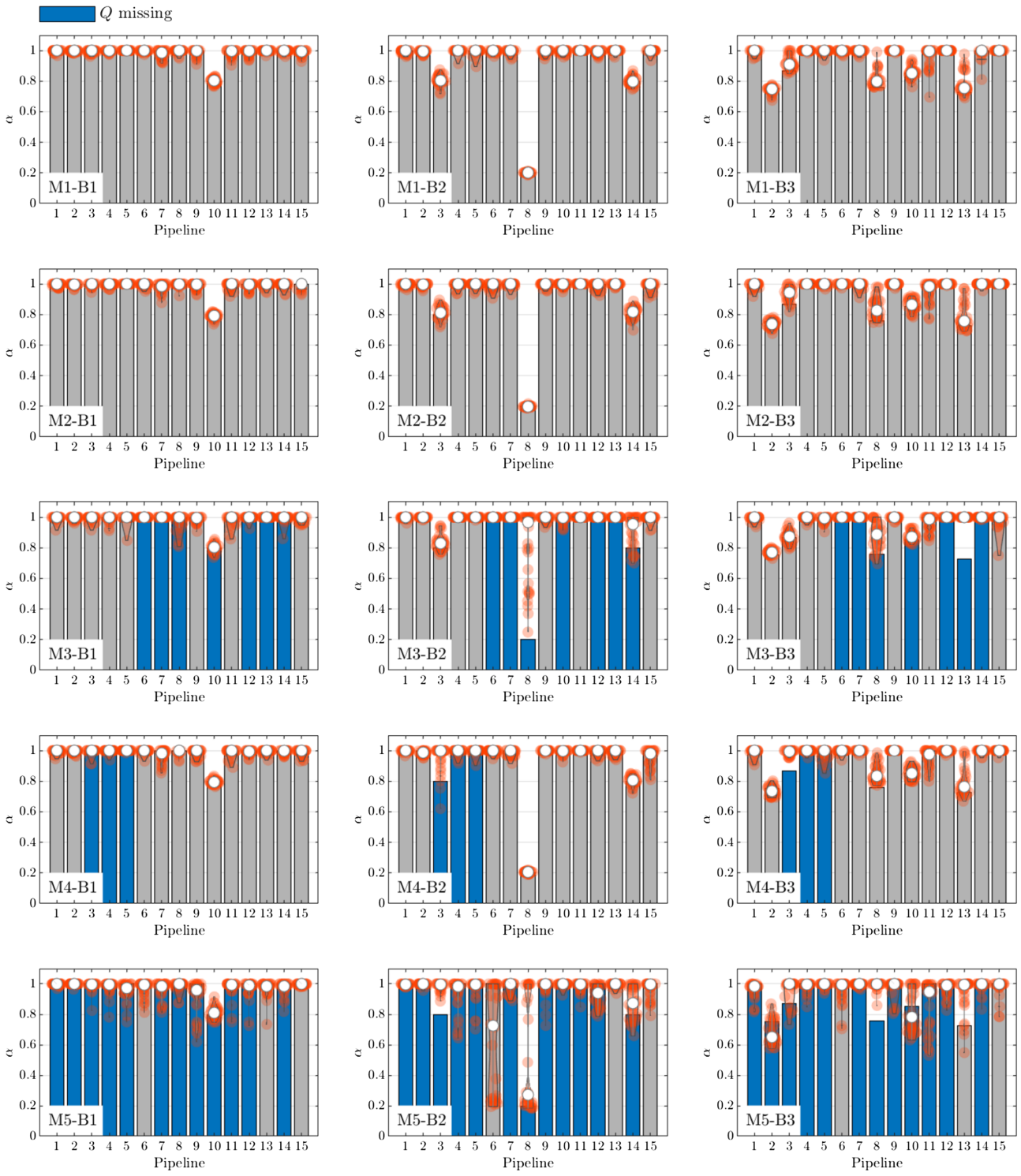

FIGURE 6 Results of 30 identifications for the fifteen scenarios. The analyses were performed with $M_Q = 5\%$ and $M_H = 10\%$. The gray bar represents the target normalized equivalent diameter α^{Ref}, the large white circles indicate the median value of the 30 identified α^{ID}, whereas the violin plots are used to show their probability density

Figures 7 and 8 clearly show that the proposed methodology is capable of identifying the restrictions with an average error that is generally has a magnitude of 5%, which is the measurement noise level that has been considered in this study.

In order to provide a synthetic result on the numerical experimentation carried out, useful to determine whether an identification (α^{ID}) may represent a restriction or a false positive, three indexes are introduced:

TABLE 6 Identification results for the restriction scenarios in Table 5

Scenario	Residual diameter	Pipeline 1	2	3	4	5	6	7	8	9	10	11	12	13	14	15
Measurement case M1																
B1	α^{Ref}	1.00	1.00	1.00	1.00	1.00	1.00	1.00	1.00	1.00	0.80	1.00	1.00	1.00	1.00	1.00
	mean (α^{ID})	0.99	0.99	0.99	0.99	1.00	0.99	0.98	0.99	0.99	0.80	0.98	0.99	0.99	0.99	0.99
	$CoV\%(\alpha^{ID})$	0.81	0.62	1.07	0.72	0.07	0.63	2.79	1.19	2.30	2.25	2.39	1.20	0.64	0.95	1.76
B2	α^{Ref}	1.00	1.00	0.80	1.00	1.00	1.00	1.00	0.20	1.00	0.80	1.00	1.00	1.00	0.80	1.00
	mean (α^{ID})	0.99	0.99	0.81	0.99	1.00	0.99	0.98	0.20	0.99	0.80	1.00	0.99	0.99	0.80	0.99
	$CoV\%(\alpha^{ID})$	1.17	1.10	4.27	1.57	2.24	0.90	1.46	2.82	1.43	1.15	0.00	1.39	0.97	3.43	1.31
B2	α^{Ref}	1.00	0.75	0.87	1.00	1.00	1.00	1.00	0.76	1.00	0.85	1.00	1.00	0.73	1.00	1.00
	mean (α^{ID})	0.99	0.74	0.92	1.00	0.99	0.99	0.99	0.81	0.99	0.86	0.96	1.00	0.78	0.99	0.99
	$CoV\%(\alpha^{ID})$	1.50	3.03	4.98	0.29	1.28	0.87	1.03	6.75	0.31	4.44	7.29	0.07	9.19	3.72	0.13
Measurement case M2																
B1	α^{Ref}	1.00	1.00	1.00	1.00	1.00	1.00	1.00	1.00	1.00	0.80	1.00	1.00	1.00	1.00	1.00
	mean (α^{ID})	0.99	0.99	0.99	0.99	1.00	0.99	0.98	0.99	0.98	0.79	0.99	0.98	0.99	0.99	0.99
	$CoV\%(\alpha^{ID})$	1.11	0.97	1.27	1.13	0.01	1.28	2.99	1.49	2.09	2.33	2.17	2.18	1.46	1.81	1.97
B2	α^{Ref}	1.00	1.00	0.80	1.00	1.00	1.00	1.00	0.20	1.00	0.80	1.00	1.00	1.00	1.00	1.00
	mean (α^{ID})	0.99	0.99	0.81	0.99	0.99	0.99	0.99	0.19	0.99	0.99	1.00	0.98	0.99	0.81	0.99
	$CoV\%(\alpha^{ID})$	0.98	1.09	4.93	1.78	1.48	2.25	1.35	3.03	1.40	1.25	0.00	2.20	0.76	4.80	2.57
B3	α^{Ref}	1.00	0.75	0.87	1.00	1.00	1.00	1.00	0.76	1.00	0.85	1.00	1.00	0.73	1.00	1.00
	mean (α^{ID})	0.99	0.74	0.93	1.00	0.99	0.99	0.99	0.84	0.99	0.86	0.95	0.99	0.79	0.99	1.00
	$CoV\%(\alpha^{ID})$	1.88	3.39	5.04	0.05	0.77	0.54	2.02	8.32	0.63	4.51	6.90	0.22	10.79	0.82	0.00
Measurement case M3																
B1	α^{Ref}	1.00	1.00	1.00	1.00	1.00	1.00	1.00	1.00	1.00	0.80	1.00	1.00	1.00	1.00	1.00
	mean (α^{ID})	0.99	0.99	0.99	0.99	0.99	1.00	1.00	0.97	0.98	0.79	0.98	0.99	0.99	0.99	0.99
	$CoV\%(\alpha^{ID})$	1.68	1.06	1.91	2.19	2.78	0.02	0.00	5.78	2.18	3.40	3.66	1.38	0.11	2.62	1.82
B2	α^{Ref}	1.00	1.00	0.80	1.00	1.00	1.00	1.00	0.20	1.00	1.00	1.00	1.00	1.00	0.80	1.00
	mean (α^{ID})	0.99	0.99	0.83	1.00	0.99	1.00	1.00	0.80	0.99	0.98	1.00	1.00	1.00	0.99	0.99
	$CoV\%(\alpha^{ID})$	0.81	0.44	6.00	0.01	0.38	0.00	0.00	31.19	1.61	2.54	0.02	0.00	0.00	12.11	2.15
B3	α^{Ref}	1.00	0.75	0.78	1.00	1.00	1.00	1.00	0.76	1.00	0.85	1.00	1.00	0.73	1.00	1.00
	mean (α^{ID})	0.99	0.77	0.87	0.99	0.98	1.00	1.00	0.88	0.99	0.88	0.96	1.00	1.00	0.99	0.98
	$CoV\%(\alpha^{ID})$	1.52	2.19	4.81	1.17	2.19	0.00	0.00	10.40	0.86	3.62	5.05	0.00	0.00	0.45	4.87

(Continues)

TABLE 6 (Continued)

Scenario	Residual diameter	Pipeline 1	2	3	4	5	6	7	8	9	10	11	12	13	14	15
Measurement case M4																
B1	α^{Ref}	1.00	1.00	1.00	1.00	1.00	1.00	1.00	1.00	1.00	0.80	1.00	1.00	1.00	1.00	1.00
	mean (α^{ID})	0.99	0.99	0.99	0.99	0.99	0.99	0.96	0.99	0.99	0.79	0.99	0.99	0.99	0.99	0.99
	$CoV\%(\alpha^{ID})$	1.29	1.05	2.25	1.20	0.29	1.41	4.48	1.74	2.43	2.01	2.76	1.57	1.37	1.36	2.21
B2	α^{Ref}	1.00	1.00	0.80	1.00	1.00	1.00	1.00	0.20	1.00	1.00	1.00	1.00	1.00	0.80	1.00
	mean (α^{ID})	0.99	0.74	0.98	0.99	1.98	0.99	0.99	0.85	1.00	0.85	0.95	0.99	0.79	0.99	0.99
	$CoV\%(\alpha^{ID})$	2.34	4.29	1.71	0.93	3.65	1.11	0.68	7.16	0.00	4.67	3.61	0.70	11.48	1.21	0.85
B3	α^{Ref}	1.00	0.75	0.87	1.00	1.00	1.00	1.00	0.76	1.00	0.85	1.00	1.00	1.00	0.73	1.00
	mean (α^{ID})	0.99	0.74	0.98	0.99	0.98	0.99	0.99	0.85	1.00	0.85	0.95	0.99	0.79	0.99	0.99
	$CoV\%(\alpha^{ID})$	2.34	4.29	1.71	0.93	3.65	1.22	0.68	7.16	0.00	4.76	6.31	0.70	11.48	1.21	0.85
Measurement case M5																
B1	α^{Ref}	1.00	1.00	1.00	1.00	1.00	1.00	1.00	1.00	1.00	1.00	0.80	1.00	1.00	1.00	1.00
	mean (α^{ID})	0.99	0.99	0.99	0.98	0.95	0.96	0.96	0.99	0.90	0.81	0.97	0.96	0.97	0.97	0.99
	$CoV\%(\alpha^{ID})$	0.70	0.66	3.36	4.60	6.42	5.43	6.04	3.36	13.30	4.88	6.48	6.98	5.44	4.55	0.66
B2	α^{Ref}	1.00	1.00	0.80	1.00	1.00	1.00	1.00	0.20	1.00	1.00	1.00	1.00	1.00	0.80	1.00
	mean (α^{ID})	0.99	0.99	0.98	0.92	0.96	0.63	0.98	0.53	0.97	0.99	0.98	0.92	0.99	0.87	0.96
	$CoV\%(\alpha^{ID})$	0.67	0.93	2.84	12.68	8.33	57.08	3.77	70.17	6.66	1.42	3.29	7.81	1.41	12.39	6.03
B3	α^{Ref}	1.00	0.75	0.87	1.00	1.00	1.00	1.00	0.76	1.00	0.85	1.00	1.00	0.73	1.00	1.00
	mean (α^{ID})	0.96	0.68	0.96	0.98	0.99	0.95	0.99	0.98	0.97	0.82	0.84	0.96	0.92	0.98	0.97
	$CoV\%(\alpha^{ID})$	5.43	11.96	7.83	3.62	1.51	8.14	0.93	2.89	6.18	16.78	20.19	5.00	13.36	3.77	6.11

Note: In the second column from the left, α^{Ref} denotes the parameters α to be identified, while mean (α^{ID}) and *CoV%* stand for the mean and coefficient of variation of the parameters α identified by the procedure, respectively.

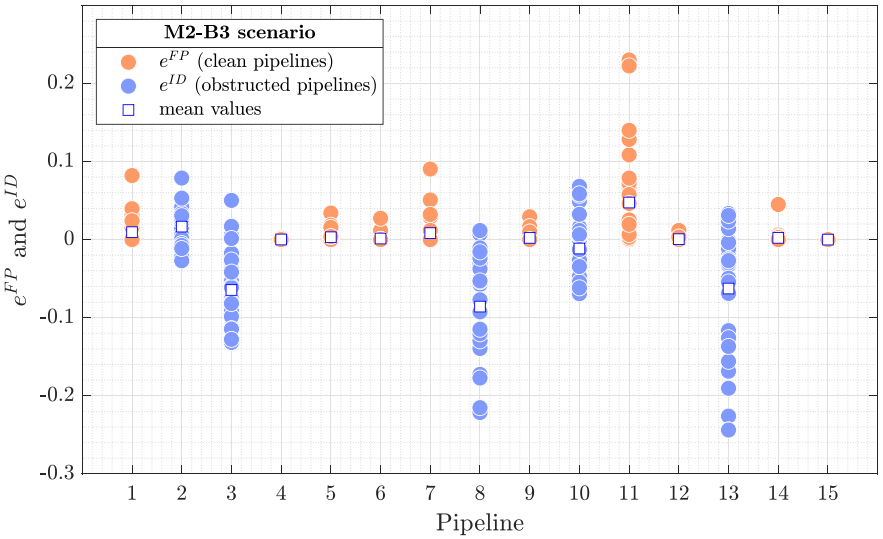

FIGURE 7 Errors e^{FP} and e^{ID} for each pipe in measurement case M2 and restriction condition B3 (Pipes 2, 3, 8, 10, and 13 are restricted)

$$I^{B}\left(\alpha^{LB},\alpha^{UB}\right)=\frac{\sum_{s}\sum_{i=1}^{15}\sum_{m=1}^{30}\mathcal{H}\left(\alpha_{s,i}^{Ref}-\alpha^{LB}\right)\cdot\mathcal{H}\left(\alpha^{UB}-\alpha_{s,i}^{Ref}\right)\cdot\mathcal{H}\left(\alpha_{s,i,m}^{ID}-\alpha^{LB}\right)\cdot\mathcal{H}\left(\alpha^{UB}-\alpha_{s,i,m}^{ID}\right)}{\sum_{s=}\sum_{i=1}^{15}30\cdot\mathcal{H}\left(\alpha_{s,i}^{Ref}-\alpha^{LB}\right)\cdot\mathcal{H}\left(\alpha^{UB}-\alpha_{s,i}^{Ref}\right)},\tag{19}$$

$$I^{FP}\left(\alpha^{LB},\alpha^{UB}\right)=\frac{\sum_{s}\sum_{i=1}^{15}\sum_{m=1}^{30}\delta\left(\alpha_{s,i}^{Ref}-1\right)\cdot\mathcal{H}\left(\alpha_{s,i,m}^{ID}-\alpha^{LB}\right)\cdot\mathcal{H}\left(\alpha^{UB}-\alpha_{s,i,m}^{ID}\right)}{\sum_{s}\sum_{i=1}^{15}30\cdot\delta\left(\alpha_{s,i}^{Ref}-1\right)},\tag{20}$$

$$I^{E}\left(\alpha^{LB},\alpha^{UB}\right)=\frac{\sum_{s}\sum_{i=1}^{15}\sum_{m=1}^{30}\delta\left(\alpha_{s,i}^{Ref}-1\right)\cdot\delta\left(\alpha_{s,i,m}^{ID}-1\right)}{\sum_{s}\sum_{i=1}^{15}30\cdot\delta\left(\alpha_{s,i}^{Ref}-1\right)},\tag{21}$$

where $\mathcal{H}(\cdot)$ is the Heaviside step function of the argument in parenthesis, $\delta(\cdot)$ is the Dirac delta function of the argument in parenthesis, and α^{LB} and α^{UB} are lower and upper bounds for α, to define a range of study. The first index, or index of restrictions I^{B}, is the percentage of cases where both α^{Ref} and α^{ID} are in the range $(\alpha^{LB},\alpha^{UB})$, normalized over the total number of cases when α^{Ref} is in such range. In other words, the coefficient I^{B} returns information on how many restrictions with α^{Ref} between α_{LB} and α_{UB} were actually identified by the procedure with an α^{ID} that lies in the same range. The second index, or false-positive index I^{FP}, has at the numerator the number of cases where the pipe is unobstructed ($\alpha_{s,i}^{Ref}=1$) and the identification result α^{ID} is between α_{LB} and α_{UB}, while the denominator indicates the total number of unobstructed pipes. Therefore, this index gives the percentage of false positives, i.e., clean pipes for which $\alpha^{LB}\leq\alpha^{ID}\leq\alpha^{UB}$. Finally, the third index I^{E} establishes how many times a clean pipe with $\alpha^{Ref}=1$ is perfectly identified. Obviously, this index can be computed only for those cases where $\alpha^{Ref}=1.0$ as indicated in Equation (21).

The values of the three indexes for various intervals of the parameter α_{LB} and α_{UB} are collected in Table 7. This table brings together the information from the identification procedure useful in deciding whether a value of α^{ID} could be related to a pipe that is actually restricted and needs additional investigations or not. For example, assuming that all measures are collected (i.e., case M1) and $\alpha^{ID}=0.86$ is the identified value for a pipe of the network examined here, it can be said that 57.33% of the times the procedure identifies actual restrictions when the result is in the range $\alpha^{ID}=0.80$ and $\alpha^{ID}=0.90$ and that there is only a 0.65% chance that it is a false positive.

In addition to the numerical application presented in this section, a numerical campaign has been carried out on many networks with different topology, taking into account data errors and missing measurements. In general, the convergence was affected by the value adopted for γ. Values of γ included in the range [10, 25] have usually led to good convergence. In particular, the value of $\gamma=17$ has shown an optimal versatility, robustness with respect to many network topologies.

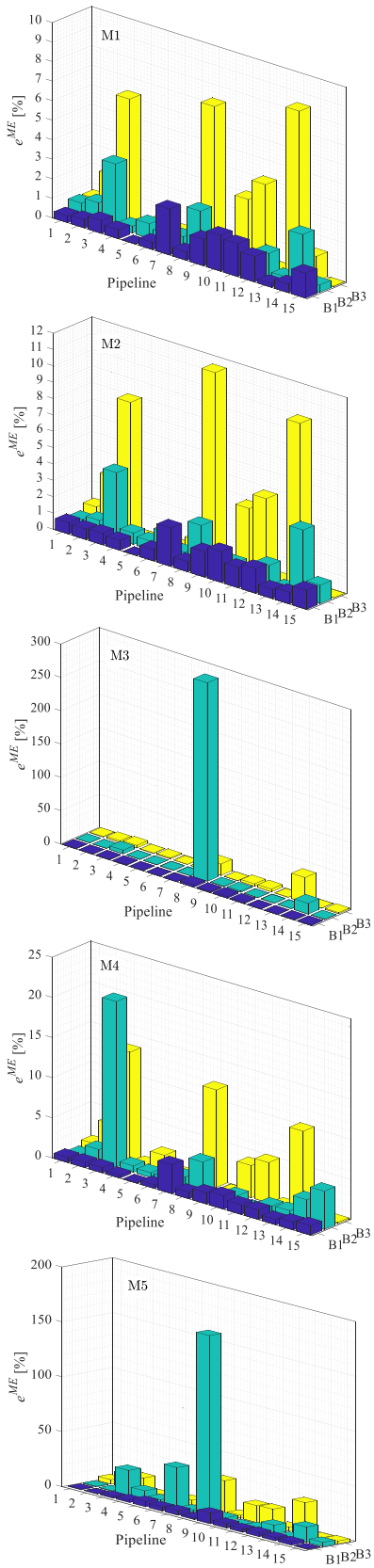

FIGURE 8 Mean relative error e^{ME} for each pipe in measurement case M1–M5 and restriction conditions B1–B3

TABLE 7 Indexes I^B, I^{FP}, and I^E for the 30 × 3 identifications for five measurement cases

Measurement case	$0.2 \leq \alpha^{ID} < 0.3$		$0.7 \leq \alpha^{ID} < 0.8$		$0.8 \leq \alpha^{ID} < 0.9$		$0.9 \leq \alpha^{ID} < 1.0$		$\alpha^{ID} = 1.0$
	I^B (%)	I^{FP} (%)	I^B (%)	I^{FP} (%)	I^B (%)	I^{FP} (%)	I^B (%)	I^{FP} (%)	I^E (%)
M1	73.33	0.00	68.33	0.00	57.33	0.65	—	33.89	65.37
M2	43.33	0.00	55.83	0.19	53.33	0.46	—	35.56	63.80
M3	3.33	0.00	34.17	0.09	56.67	1.20	—	23.33	75.37
M4	76.67	0.00	54.17	0.09	38.00	1.70	—	30.28	67.96
M5	40.00	1.02	16.67	2.96	20.67	5.83	—	51.94	36.67

Note: For $0.9 \leq \alpha^{ID} < 1.0$, no values of I^B are provided because such situation does not appear in the considered scenarios.

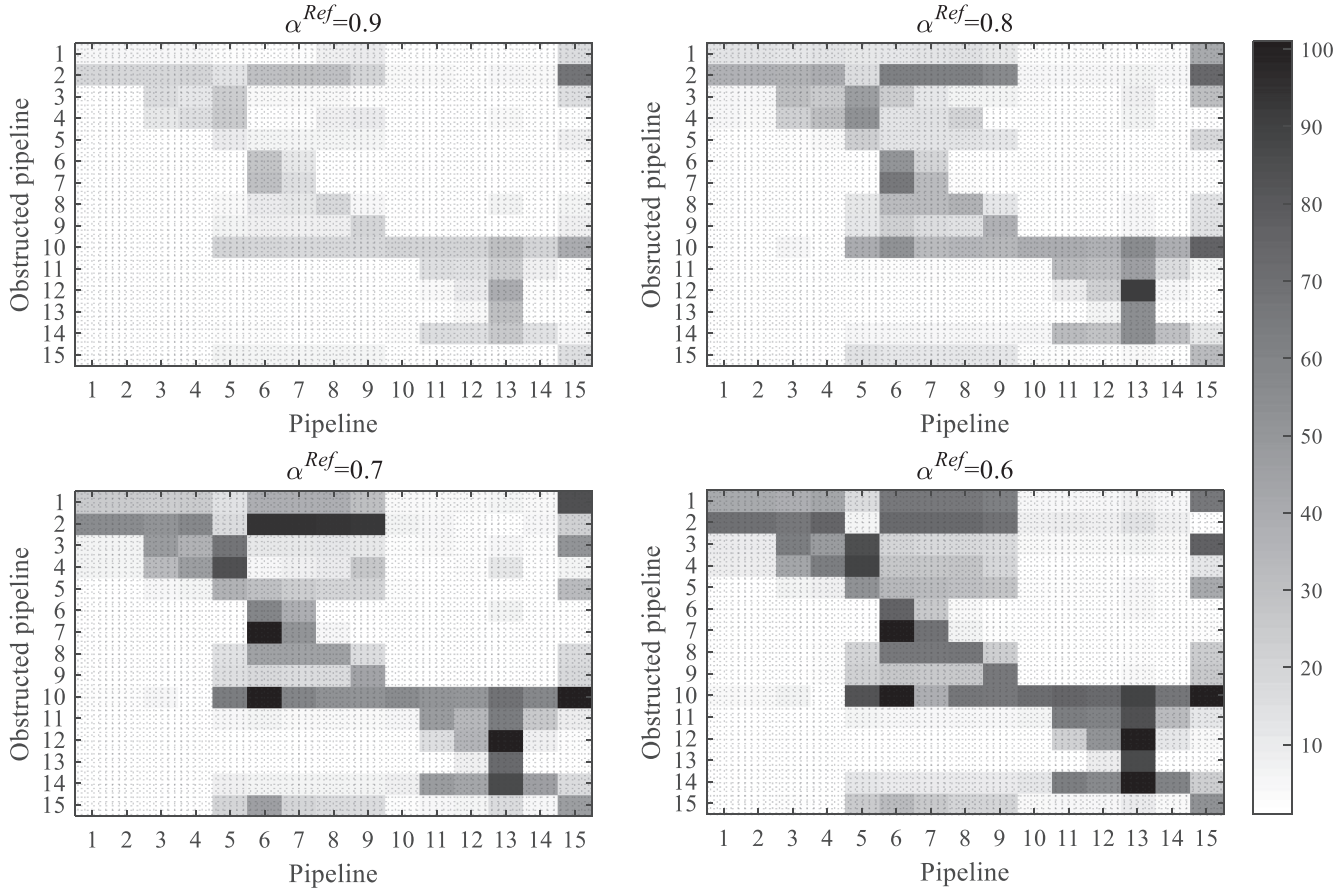

FIGURE 9 Percentage change in the volumetric flow rate in the pipe of the network for a given pipe occluded with different α^{Ref}

3.5 | Network sensitivity analysis

The number of required measurements is, as is well known, a critical aspect of any identification procedure. Therefore, techniques aimed at evaluating the minimum number of measurements sufficient to properly solve the inverse problem are of interest. For a selected number of measures to be acquired, these techniques allow the best positioning of the sensors. In this context, the measures of flow rate and pressure head which appear to be most sensitive to a given occlusion can be highlighted through simple recursive direct analyses. In particular, Figure 9 presents the following quantity:

$$\Delta Q_i(\alpha^B, \ ) = \left| \frac{Q_i^B(\alpha^B, \ ) - Q_i}{Q_i} \right| \cdot 100, \tag{22}$$

where Q_i is the flow rates in the pipelines of the network computed in the absence of restrictions, whereas $Q_i^B(\alpha^B, \tilde{i})$ is the flow rates computed by considering only one restriction at pipe with normalized equivalent diameter $\alpha^{Ref} = \alpha^B$. Values of α^B equal to 0.9, 0.8, 0.7, and 0.6 have been considered. For instance, it can be seen that a restriction in Pipe 7 generates significant variations of flows only in Pipes 6 and 7, for any value of α^B, whereas a restriction in Pipe 10 induces a significant change of flow in Pipes 5–15. It follows that placing a sensor to measure the flow in Pipe 5 can be useful to detect a restriction in Pipeline 10, while it will not provide information to identify a restriction in Pipe 7. Instead, placing a sensor in Pipe 6 provides information to identify restrictions in Pipes 7 and 10. In addition, it can be noted that while a restriction in Pipe 10 generates a change of flow rate in several pipes of the network, a restriction in Pipe 8 or 13 does not. In fact, pipe 10 was properly identified in all the considered cases, even with several missing measurements, whereas Pipes 8 and 13 were misclassified in some cases (see Figure 6).

Similarly, the variation of pressure heads at the nodes is represented in Figure 10 for the same values of α^B, i.e., 0.9, 0.8, 0.7, and 0.6:

$$\Delta H_n(\alpha^B, \ ) = \left| \frac{H_n^B(\alpha^B, \ ) - H_n}{H_n} \right| \cdot 100, \tag{23}$$

where H_n is the nodal pressure heads computed for the pipe network without restrictions, whereas H_n^B is the nodal pressure heads computed by considering a restriction in pipe with $\alpha^{Ref} = \alpha^B$. In the same Figure 10, the red circles denote the reservoirs in which the pressure is fixed and not affected by the presence of restrictions.

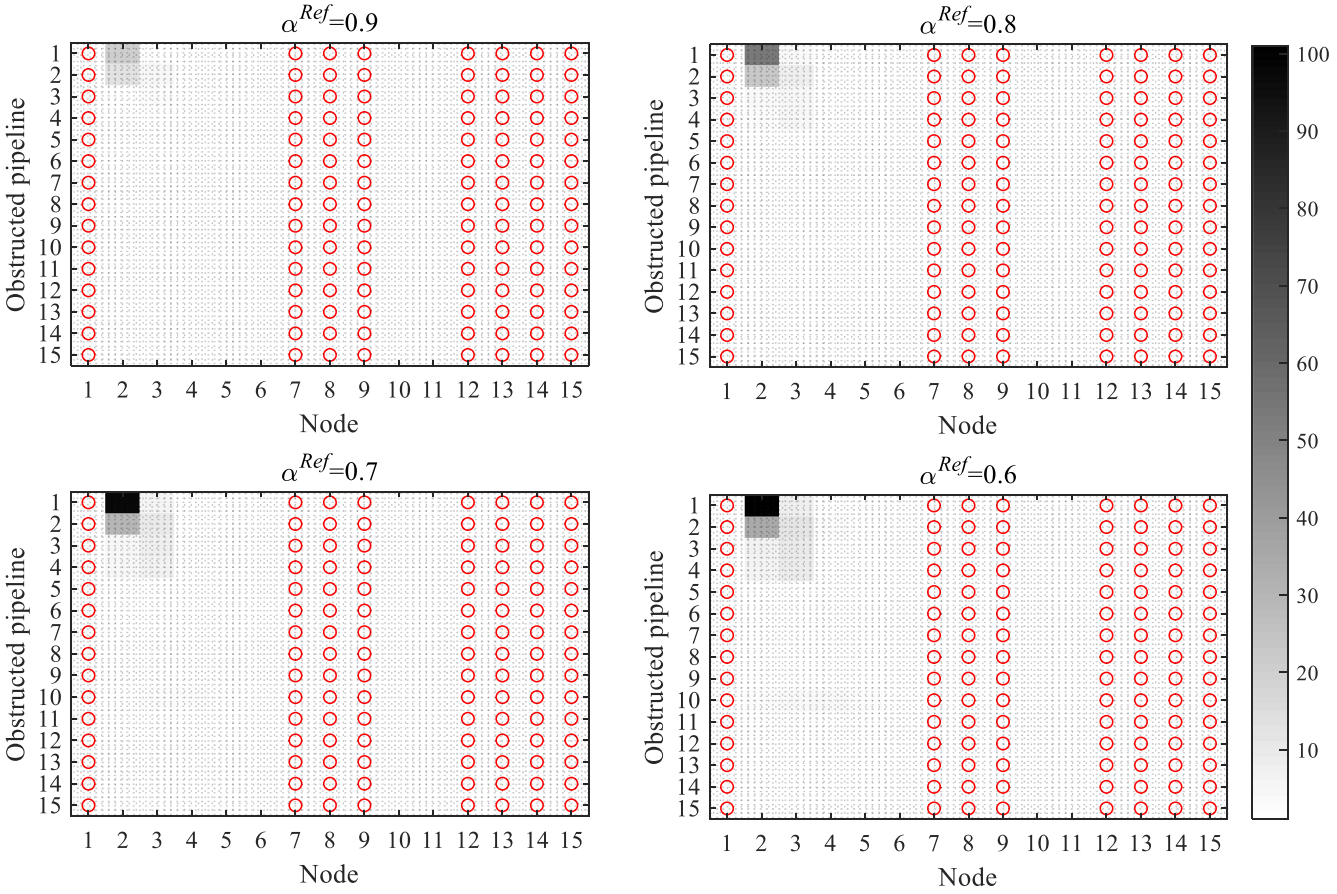

FIGURE 10 Percentage change in pressure in the various nodes of the network for a given pipe occluded (obstructed pipe) with α^{Ref}. Red circles indicate nodes in which the pressure is imposed (reservoir) and does not vary

From these two figures, it is easy to infer which pipes are most sensitive to the presence of restrictions in the network. This type of analysis can be useful not only in the design of the experiment but also in the management of monitoring actions. For example, if the identification procedure indicates the presence of a restriction in a certain pipe, through this analysis, it is possible to further highlight which flow rates and pressure heads are important to monitor, in order to confirm the presence of a restriction, by observing changes in time related to the growth of the restriction as well as to safeguard the operative condition of the pipe network by establishing levels of risk based on the restriction dimension.

4 | CONCLUSIONS

A procedure to identify partial restrictions in pipe networks using steady-state data has been proposed. The procedure uses a FEM coupled with a GA optimization. By leveraging measures of pressure head at nodes and of flow rates in the pipes, the residual equivalent diameter can be estimated for each pipe in the network. In this description of the procedure, the experimental data have been replaced by pseudo-experimental data. Numerical simulations on 15 different restriction scenarios are discussed on a 15-pipe and 15-node network carrying crude oil, taking data uncertainty (5% level error on flows and 10% on pressure heads) into account. The obtained results show a very good agreement between reference and detected equivalent residual diameters, with average errors generally close to the measurement noise. The procedure has also shown a good sensitivity in the detection of restricted pipes for which flow measures are not collected directly, but inferred through conservation of mass.

The approach based on the equivalent residual diameter allows to detect restricted or obstructed pipe and gives a general information on their overall restriction level but cannot characterize the actual size of the restriction (length and residual diameter). For restriction characterization, multirate, transients, or coupled frictional and mass balance methods are needed. However, this economical and nondestructive method, if applied to the entire pipe network, could be useful to identify the obstructed pipe that require further inspections.

The proposed methodology requires measurements across the network, which nowadays tend to be readily available mostly for oil and gas pipelines. However, there is a general trend to increase the amount of data collected in all infrastructure systems, driven by the data revolution, the advancements in sensor technology, and their price reduction. For this reason, it is probable that in a near future, it will be possible to apply the same technique also to other infrastructure networks, such as water and waste water systems.

NOTATION

$\|\cdot\|_{L2}$	L^2 norm
A	element-wise assembly operator
c	normalized friction coefficient
D	diameter of the pipe or segment
$\hat{D}$	"equivalent diameter" of the pipe
$\tilde{D}$	residual diameter in the restricted portion
e	roughness of a pipe or pipe's portion
e^{ID}	identification error
e^{FP}	false positives error
e^{ME}	mean error
f	friction factor
g	gravitational acceleration
H	pressure head
$\mathbf{H}$	vector of the pressure heads of all nodes in a network
h_L	head loss of a pipe or pipe's portion
	index of the only restricted pipe in the network
I^B	index of restrictions
I^{FP}	index of false-positive
I^E	index of perfectly clean identified pipe
J	fitness function
k	frictional loss coefficient

L	length of the pipe or segment
$\tilde{L}$	length of a restricted portion
M_H	pressure head noise level (simulated measurement error)
M_Q	discharge noise level (simulated measurement error)
n_{inl}, n_{out}	inlet and outlet nodes of a pipe
N_I	number of individuals in a GA generation
N_P	number of pipe in the network
N_N	number of nodes in the network
N_H	number of measured pressure heads
N_Q	number of measured flow rates
$N_{s,\,i}$	number of segments along pipe i
Q	discharge, volumetric flow rate
$\mathbf{Q}_E$	vector of the external inlets and outlets of all nodes in a network
$\mathbf{Q}_I$	vector of the internal flow of all nodes in a network
$\mathbf{R}$	global vector of residuals
Re	Reynolds number in a pipe or pipe's portion
V	fluid speed in a pipe or pipe's portion
x	nodal coordinate
y	nodal coordinate
z	node elevation, geodetic height
α	normalized "equivalent diameter"
$\boldsymbol{\alpha}$	global vector of normalized "equivalent diameters"
γ	penalty factor
Δh	hydraulic grade line, head loss
Φ_H	pressure head discrepancy function
Φ_Q	discharge discrepancy function
μ	fluid dynamic viscosity in a pipeline or pipeline's portion
ρ	fluid density in a pipeline or pipeline's portion
τ	fluid temperature in a pipeline or pipeline's portion
ξ	random variable representing the measurement error on discharge
η	random variable representing the measurement error on pressure head
$\mathcal{H}(\cdot)$	Heaviside step function
$\delta(\cdot)$	Dirac delta function
subscript b	index of the blockage
subscript i	index of the pipeline
subscript j	index of the pipeline segment
subscript ν	summation index
subscript m	index of the analysis made with a sample of the random measurement noise
subscript n	index of the network node
subscript r	index of the iterative step
subscript s	index of the scenario $\in \{\text{M1, M2, M3, M4, M5}\} \times \{\text{B1, B2, B3}\}$
subscript w	index of the trial solution, i.e., individual in the GA procedure
superscript B	index of the restriction
superscript exp	experimental or pseudo-experimental data
superscript ID	result of the identification process
superscript LB, UB	lower and upper bound values
superscript Ref	reference value
superscript sim	simulated data
superscript T	transposed

ACKNOWLEDGMENT

The authors wish to acknowledge the Ente Nazionale Idrocarburi - Eni SpA (Italian Hydrocarbon Company) for supporting the research effort that led to the presented results.

AUTHOR CONTRIBUTION STATEMENT

Matteo Mazzotti: Conceptualization, Methodology, Software, Visualization, Validation, Writing - Original draft preparation.

Mohanad Khazaali: Conceptualization, Software, Visualization, Writing - Reviewing and Editing.

Paolo Bocchini: Supervision, Conceptualization, Methodology, Resources, Funding-acquisition, Writing - Reviewing and Editing.

Alberto Di Lullo: Conceptualization, Validation, Writing - Reviewing and Editing.

Alessandro Marzani: Supervision, Conceptualization, Methodology, Resources, Funding-acquisition, Project management, Writing - Reviewing and Editing.

ORCID

Matteo Mazzotti https://orcid.org/0000-0002-3835-7887
Mohanad Khazaali https://orcid.org/0000-0002-8803-7603
Paolo Bocchini https://orcid.org/0000-0002-5685-2283
Alessandro Marzani https://orcid.org/0000-0001-7697-6729

REFERENCES

1. Marshall GR. Cleaning the valhall offshore oil pipeline Proc. SPE Production Engineering 5; 1990:275-278.
2. Chen, NH. An explicit equation for friction factor in pipe. *Ind Eng Chem Fundam*. 1979;18(3):296-297.
3. Scott, SL, Satterwhite, LA. Evaluation of the backpressure technique for blockage detection in gas flowlines. *J Energy Res Technol*. 1998; 120(1):27-31.
4. Hoffmann R, Amundsen L. Single-phase wax deposition experiments. *Energy Fuels*. 2010;24(2):1069-1080.
5. Scott, SL, Yi, J. Flow testing methods to detect and characterize partial blockages in looped subsea flowlines. *J Energy Res Technol*. 1999; 121(3):154-160.
6. Chen, XT, Butler, T, Volk, M, Brill, JP. Techniques for measuring wax thickness during single and multiphase flow Proc. SPE Annual meeting, San Antonio TX; 1997.
7. Guillén M, Dulhoste J-F, Besançon G, Santos R. Study of a flow model for detection and location of leaks and obstructions in pipes 9th International Conference on Modeling, Optimization & Simulation; 2012; Bordeaux, France.
8. Besançon G, Guillén M, Dulhoste J-F, Santos R, Scola IR. Pipeline partial blockage modeling and identification. *IFAC Proc Volumes*. 2013;46(11):730-735. 11th IFAC Workshop on Adaptation and Learning in Control and Signal Processing.
9. Ling K, Xingru W, Zheng S. A new method to detect partial blockage in gas pipelines. *Oil and Gas Facilities*. 2016;5(05):1-7.
10. Razvarz S, Jafari R, Gegov A. *Flow modelling and control in pipeline systems - a formal systematic approach*. Cham: Springer; 2020.
11. Jafari R, Razvarz S, Vargas-Jarillo C, Gegov A. Blockage detection in pipeline based on the extended kalman filter observer. *Electronics*. 2020;9(1):91.
12. Ma J, Lowe MJS, Simonetti F. Feasibility study of sludge and blockage detection inside pipes using guided torsional waves. *Meas Sci Technol*. 2007;18(8):2629-2641.
13. Guan R, Lu Y, Duan W, Wang X. Guided waves for damage identification in pipeline structures: A review. *Struct Control Health Monit*. 2017;24(11):e2007.
14. Wan C, Mita A, Kume T. An automatic pipeline monitoring system using sound information. *Struct Control Health Monit*. 2010;17(1): 83-97.
15. Meniconi S, Brunone B, Ferrante M, Massari C. Potential of transient tests to diagnose real supply pipe systems: What can be done with a single extemporary test. *J Water Res Plan Manag*. 2011;137(2):238-241.
16. Meniconi S, Brunone B, Ferrante M. Water-hammer pressure waves interaction at cross-section changes in series in viscoelastic pipes. *J Fluids Struct*. 2012;33:44-58.
17. Pernía AM, Mayor HA, Prieto MJ, Villegas PJ, Martínez JA, Martín-Ramos JA. Estimation of blockage position, geometry, and solidity in molten salt pipelines. *Sensors*. 2020;20(12):3490.
18. Abdullahi M, Oyadiji SO. Simulation and detection of blockage in a pipe under mean fluid flow using acoustic wave propagation technique. *Struct Control Health Monit*. 2020;27(4):e2449.
19. Adewumi, MA, Eltohami, ES, Solaja, A. Possible detection of multiple blockages using transients. *J Energy Res Technol*. 2003;125(2): 154-159.
20. Wang, XJ, Lambert, MF, Simpson, AR. Detection and location of a partial blockage in a pipeline using damping of fluid transients. *J Water Res Plan Manag*. 2005;131(3):244-249.
21. Mohapatra, PK, Chaudhry, MH, Kassem, AA, Moloo, J. Detection of partial blockages in a branched piping system by the frequency response method. *J Fluids Eng*. 2006;128(5):1106-1114.
22. Lee, PJ, Vítkovský, JP, Lambert, MF, Simpson, AR, Liggett, JA. Discrete blockage detection in pipelines using the frequency response diagram: Numerical study. *J Hydraul Eng*. 2008;134(5):658-663.

23. Sattar A, Chaudhry M, Kassem A. Partial blockage detection in pipelines by frequency response method. *J Hydraul Eng*. 2008;134(1): 76-89.
24. Colombo AF, Lee P, Karney BW. A selective literature review of transient-based leak detection methods. *J Hydro-environ Res*. 2009;2(4): 212-227.
25. Ghazali MF, Beck SBM, Shucksmith JD, Boxall JB, Staszewski WJ. Comparative study of instantaneous frequency based methods for leak detection in pipeline networks. *Mech Syst Sig Process*. 2012;29(0):187-200.
26. Duan H-F, Lee PJ, Kashima A, Lu J, Ghidaoui MS, Tung Y-K. Extended blockage detection in pipes using the system frequency response: Analytical analysis and experimental verification. *J Hydraul Eng*. 2013;139(7):763-771.
27. Hanmaiahgari PR, Elkholy M, Riahi-Nezhad CK. Identification of partial blockages in pipelines using genetic algorithms. *Saādhanā*. 2017;42(9):1543-1556.
28. Duan HF, Lee PJ, Che TC, Ghidaoui MS, Karney BW, Kolyshkin AA. The influence of non-uniform blockages on transient wave behavior and blockage detection in pressurized water pipelines. *J Hydro-environ Res*. 2017;17:1-7.
29. Scola IR, Besançon G, Georges D. Blockage location in pipelines using an implicit nonlinear finite-difference model optimization. *IFAC-PapersOnLine*. 2018;51(24):935-940. 10th IFAC Symposium on Fault Detection, Supervision and Safety for Technical Processes SAFEPROCESS 2018.
30. Gurav S, Kumar P, Ramshankar G, Mohapatra PK, Srinivasan B. Machine learning approach for blockage detection and localization using pressure transients 2020 IEEE International Conference on Computing, Power and Communication Technologies (GUCON); 2020:189-193.
31. Brunone B, Capponi C, Meniconi S. Design criteria and performance analysis of a smart portable device for leak detection in water transmission mains. *Measurement*. 2021;183:109844.
32. Mantegazza T, Di Lullo A, Bocchini P, Marzani A. Methodology for the identification of blockages in pipe-networks for fluids. Patent n. H10084 deposited by ENI SpA on May 15, 2012 in Italy; 2012.
33. Bocchini P, Marzani A, Karamlou A. Blockage Detection in Pipeline Networks for Gas and Oil. *Shale Energy Engineering 2014*: American Society of Civil Engineers; 2014:676-683.
34. Goldberg DE. *Genetic algorithms in search, optimization, and machine learning*: Addison-Wesley Professional; 1989.
35. Chou, JH, Ghaboussi, J. Genetic algorithm in structural damage detection. *Comput Struct*. 2001;79(14):1335-1353.
36. Bocchini, P, Viola, E. Identification of damaged bars in three-dimensional redundant truss structures by means of genetic algorithms. *Key Eng Mater*. 2007;348-349:229-232.
37. Meruane Naranjo V, Heylen W. Damage detection by a real-parameter hybrid genetic algorithm. In: Proceedings of the European Workshop on Structural Health Monitoring; 2008:1073-1080.
38. Kokot, S, Zembaty, Z. Vibration based stiffness reconstruction of beams and frames by observing their rotations under harmonic excitations - numerical analysis. *Eng Struct*. 2009;31(7):1581-1588.
39. Viola E, Bocchini P. Non-destructive parametric system identification and damage detection in truss structures by static tests. *Struct Infrastruct Eng*. 2013;9(5):384-402.
40. Mao Q, Mazzotti M, DeVitis J, Braley J, Young C, Sjoblom K, Aktan E, Moon F, Bartoli I. Structural condition assessment of a bridge pier: A case study using experimental modal analysis and finite element model updating. *Struct Control Health Monit*. 2019;26(1):e2273.
41. Mohtar RH, Bralts VF, Shayya WH. A finite element model for the analysis and optimization of pipe networks. *Am Soc Agric Eng*. 1991; 34(2):393-401.
42. Swamee, PK, Sharma, AK. *Design of water supply pipe networks*. Hoboken: John Wiley and Sons; 2008.
43. NIST Chemistry WebBook. National Institute of Standards and Technology. Standard Reference Database 69. https://webbook.nist.gov/
44. Reddy, JN. *An introduction to nonlinear finite element analysis*: Oxford University Press; 2004.
45. Coello Coello, CA, Lamont, GB, Van Veldhuizen, DA. *Evolutionary algorithms for solving multi-objective problems*. 2nd ed. New York: Springer; 2007.
46. Crane Co. Engineering Division. *Flow of fluids: through valves, fittings, and pipe*. New York: CRANE; 1982.

How to cite this article: Mazzotti M, Khazaali M, Bocchini P, Di Lullo A, Marzani A. Restrictions and obstructions detection in pipe networks using incomplete and noisy flow and pressure steady-state measurements. *Struct Control Health Monit*. 2022;29(1):e2854. doi:10.1002/stc.2854